BASIC SCIENCE

Deficiency of aldose reductase attenuates inner retinal neuronal changes in a mouse model of retinopathy of prematurity

Zhongjie Fu[1] · Shen Nian[1] · Suk-Yee Li[1] · David Wong[1,3] · Sookja K. Chung[2,3] ·
Amy C. Y. Lo[1,3,4]

Abstract Retinopathy of prematurity (ROP) is a leading cause of childhood blindness where vascular abnormality and retinal dysfunction are reported. We showed earlier that genetic deletion of aldose reductase (AR), the rate-limiting enzyme in the polyol pathway, reduced the neovascularization through attenuating oxidative stress induction in the mouse oxygen-induced retinopathy (OIR) modeling ROP. In this study, we further investigated the effects of AR deficiency on retinal neurons in the mouse OIR. Seven-day-old wild-type and AR-deficient mice were exposed to 75 % oxygen for 5 days and then returned to room air. Electroretinography was used to assess the neuronal function at postnatal day (P) 30. On P17 and P30, retinal cytoarchitecture was examined by morphometric analysis and immunohistochemistry for calbindin, protein kinase C alpha, calretinin, Tuj1, and glial fibrillary acidic protein. In OIR, attenuated amplitudes and delayed implicit time of a-wave, b-wave, and oscillatory potentials were observed in wild-type mice, but they were not significantly changed in AR-deficient mice. The morphological changes of horizontal, rod bipolar, and amacrine cells were shown in wild-type mice and these changes were partly preserved with AR deficiency. AR deficiency attenuated the Müller cell gliosis induced in OIR. Our observations demonstrated AR deficiency preserved retinal functions in OIR and AR deficiency could partly reduce the extent of retinal neuronal histopathology. These findings suggested a therapeutic potential of AR inhibition in ROP treatment with beneficial effects on the retinal neurons.

Keywords Aldose reductase · Retinal neurons · Retinopathy of prematurity · Oxygen-induced retinopathy

Zhongjie Fu and Shen Nian contributed equally to this work.

✉ Amy C. Y. Lo
amylo@hkucc.hku.hk

1   Department of Ophthalmology, Li Ka Shing Faculty of Medicine, The University of Hong Kong, Hong Kong, SAR, China

2   Department of Anatomy, Li Ka Shing Faculty of Medicine, The University of Hong Kong, Hong Kong, SAR, China

3   Research Center of Heart, Brain, Hormone and Healthy Aging, Li Ka Shing Faculty of Medicine, The University of Hong Kong, Hong Kong, SAR, China

4   L4-04, 4/F, Hong Kong Jockey Club Building for Interdisciplinary Research, 5 Sassoon Road, Pokfulam, Hong Kong

Introduction

Retinopathy of Prematurity (ROP), which was first described in the 1940s, is a common blinding disease in premature babies with long term disability and diminished quality of life, creating a big burden to the aging society when they get old [1]. It is regarded as a vascular disease characterized first by vaso-obliteration and then pathological angiogenesis, excessive growth of blood vessels on the surface of the retina in response to the combined effects of immature retinal vasculature, and high levels of supplemental oxygen for neonatal clinical care [2–4]. In addition to the most well-known pathological retinal angiogenesis of this disease [2], reduced visual acuity, and neuronal dysfunction have also been observed in infants and children with a history of ROP [5, 6]. Alterations of electroretinographic (ERG) responses, including lower saturated amplitude, decreased sensitivity, and prolonged deactivation of rod photoreceptors have been observed, and these deficits appear to persist long even after ROP has been

resolved [7–9]. Moreover, attenuated post-receptor responses are also present, although these deficits can be improved in children with a history of mild ROP, they stay in severe ROP [7, 9–11]. In rat or mouse models of oxygen-induced retinopathy (OIR) to mimic human ROP, altered ERG responses for rods and post-receptors, disrupted rod outer segment, morphological or neurochemical changes in horizontal, bipolar, or amacrine cells have been reported [3–5, 7, 12–14]. However, current treatments for ROP such as laser therapy, vitrectomy or VEGF inhibitor Bevacizumab, mainly focus on the pathological retinal angiogenesis [15–17]. Therefore, there is a great need to also investigate the long-term impact on retinal neurons of the potential therapeutic targets, which may demonstrate beneficial effects on attenuating the pathological retinal angiogenesis.

Oxidative stress has been highly implicated to contribute to the pathogenesis of ROP. Previous clinical studies have demonstrated increased oxidative stress in preterm infants [18]. Antioxidant supplement vitamin E has been shown to reduce the development and progression of ROP [19]. These observations suggest that targeting oxidative stress would be an efficient therapeutic approach in ROP treatment. Aldose reductase (AR) is the first enzyme in the polyol pathway for reducing glucose to sorbitol, using NAD(P)H as a cofactor [20]. Increased AR activity contributes to oxidative stress [21–26]. In the mouse retina, AR deficiency or inhibition of AR activity has been shown to reduce ischemia-induced oxidative stress [20, 27]. In our previous studies, genetic deletion or pharmacological inhibition of AR reduced the retinal vascular changes including central vaso-obliteration and neovascularization with reduced induction of oxidative stress in the mouse model of OIR [27]. In the current studies, we aimed to further evaluate the effects of genetic deletion of AR on retinal neuronal changes at both functional and cellular levels. We hypothesize that AR deficiency helps protect the retinal neurons in OIR.

Methods

Animals

All experimental and animal handling procedures were in accordance with the ARVO Statement for the Use of Animals in Ophthalmic and Vision Research. The use of animals was conducted according to the requirements of the Cap. 340 Animals (Control of Experiments) Ordinance and Regulations, and all relevant legislation and Codes of Practice in Hong Kong, and was approved by the Faulty Committee on the Use of Live Animals in Teaching and Research in The University of Hong Kong (CULATR 1691–08 and 2423–11).

Animal model of OIR

OIR was induced in wild-type (WT) and AR-deficient (AR$^{-/-}$) mice [28]. Neonatal mice and their nursing dams were exposed to a 75 % oxygen (PRO-OX110 chamber controller; Biospherix Ltd, NY, USA) at postnatal day seven (P7), returned to room air on P12, and kept until P17 [29]. The hyperoxia from P7 to P12 induces retinal blood vessel regression, and the relative hypoxia-induced neovascularization reaches maximum on P17 [30]. During the exposure to high oxygen, soda lime was placed inside the chamber to serve as CO_2 quencher. To reduce the runty phenotype, the litter size was limited to seven or eight pups for each mother [30]. AR$^{-/-}$ mice were observed to breed well, and the weight of pups on P7 (~4 g) and P17 (~6 g) was identical to that of WT mouse pups with limited litter size in OIR.

Samples were collected on P17 and P30. Both eyes were enucleated and fixed in 4 % paraformaldehyde (PFA) in phosphate buffered saline (PBS; 0.01 M; pH 7.4) overnight at 4 °C and then dehydrated in a graded series of ethanol and chloroform. Subsequently, eyeballs were infiltrated with paraffin for 3 hours (new paraffin changed every hour) and embedded. Sagittal sections (6 μm) were cut through the cornea parallel to the optic nerve using a microtome (Microm HM 315R, Heidelberg, Germany).

Assessment of retinal function by electroretinogram

Scotopic flash electroretinogram (ERG) was recorded from mice on P30 to assess retinal function. Before ERG measurement, mice were dark-adapted overnight and anesthetized with a mixture of Ketamine (50 mg/kg; Alfasan International, Woerden, The Netherlands) and Xylazine (0.5 mg/kg; Alfasan International, Woerden, The Netherlands). The eyes were further treated with 0.5 % proparacaine hydrochloride (Alcon, Alcon-Couvreur, Belgium) for topical analgesia and pupils were dilated with 1% Mydricyl (Alcon, Alcon-Couvreur, Belgium). The ERG signals were recorded by placing a gold active electrode on the cornea as well as a reference and a ground electrode in the forehead and tail region, respectively. All operations were performed under dim red light, and mice were kept warm on a heating pad during the ERG recording. Rod and cone responses were elicited by the single white flashes of intensity at 3 cd·s/m^2 generated from the Color Dome Ganzfeld System (Diagnosys, Lowell, MA). Each flash lasted for 4 ms and the flash interval was 10 s. All ERG signals were amplified automatically by the system. For a-wave and b-wave, responses were recorded with a band-pass filtered from 0.3 to 300 Hz; for oscillatory potentials (OPs), responses were recorded with a band-pass filtered from 100 to 300 Hz. The sum of only OP2 to OP4 amplitudes was analyzed due to the potential of OP1 contaminated by the a-wave [31]. Fifteen readings from two eyes for each mouse were averaged and

analyzed using the Epsion V5 software incorporated with the system.

Measurement of retinal layer thickness

Three sagittal sections with an optic nerve head for each eye were selected and stained with hemotoxylin and eosin (H&E). Two images from the same section were captured for central and mid-peripheral retinal areas with one from each side of the optic nerve, using an upright microscope with 400X magnification (Eclipse 80i, Nikon, Japan). The central retinal area was defined as ~100 μm away from the optic nerve; the mid-peripheral retinal area was defined as the middle area between optic nerve and the end of the retina on each side. Outer nuclear layer (ONL), inner nuclear layer (INL) and inner plexiform layer (IPL) thicknesses were then measured using Spot Advanced software (SPOT™ Imaging Solutions, Sterling Heights, USA).

Immunohistochemistry (IHC) for various retinal neurons and glial cells

Deparaffinized retinal sagittal sections were subjected to antigen retrieval by incubation with proteinase K (20 μg/ml in PBS) for 4 min at room temperature. Sections were blocked with goat or donkey serum (Vector Laboratories Inc.) and incubated with primary antibodies rabbit anti-PKCα (rod bipolar cell marker, 1:500; sc-208, Santa Cruz Biotechnology), goat anti-calretinin (amacrine cell marker, 1:1000; sc-11644, Santa Cruz Biotechnology), mouse anti-Tuj1 (retinal ganglion cell marker, 1:1000; MRB-435P, Convance), and rabbit anti-glial fibrillary acidic protein (GFAP 1:500, Dako, Denmark), respectively, overnight at 4 °C. For rabbit anti-calbindin (horizontal cell marker, 1:500; AB1778, Chemicon) staining, sections were incubated for 72 h at 4 °C. Signals were visualized by reacting with corresponding secondary antibodies Alexa Fluor® 488 donkey anti-goat IgG (1:500, A-11055, Molecular Probes, Invitrogen), or Alexa Fluor® 568 goat anti-rabbit IgG (1:500; A-11011, Molecular Probes, Invitrogen), or Alexa Fluor® 568 goat anti-mouse IgG (1:500, A-21134, Molecular Probes, Invitrogen), respectively, for 60 min at room temperature. The sections were washed with PBS and counterstained with DAPI (0.1 μg/ml in PBS, D9564, Sigma). The immunoreactivity was examined using an upright microscope with 400X magnification (Eclipse 80i, Nikon, Japan). For horizontal and rod bipolar cells, a scoring system was used according to previous studies [27, 32, 33]. Briefly, the slides for the same immunostaining at each time point were examined at the same time under the microscope with the same light exposure intensity. The

scoring was done within 2 h. To minimize the potential bias, all the slides were re-coded and the examiners were blinded while performing the scoring. Based on the intensity and location of the staining, score one was assigned for the weakest immunoreactivity and discrete alignment of cell bodies, and score five represented the strongest immunoreactivity and evidently located cell bodies. For calretinin-positive amacrine cells in INL and Tuj1-positive RGCs in a ganglion cell layer (GCL), the number of cell bodies was counted and compared between the two genotypes. Representative images were taken from the central retinal areas of retinal sections with 400X magnification (Eclipse 80i, Nikon, Japan) using the same exposure of light intensity and time.

Statistical analysis

All experiments and analyses were performed in a double-blinded manner. The immunohistochemical investigations for all retinal sections using the same antibody were performed in one single experiment to eliminate inter-experiment errors and variation. One-way ANOVA and Bonferroni's multiple comparisons test, Kruskal-Wallis test, and Dunn's multiple comparison test were used for comparison of results as specified in the figure legends (Prism v5.0, GraphPad Software Inc., San Diego, CA). Statistically significant difference was set at $p<0.05$. Data was presented as mean±SEM.

Results

Preservation of retinal neuronal function in $AR^{-/-}$ mice

Scotopic ERG was performed to investigate the effect of OIR on neuroretinal function in WT and $AR^{-/-}$ mice on P30. Representative ERG waveforms recorded from room air and OIR retinae in both genotypes were demonstrated in Fig. 1b. Under room air, the ERG waveforms were very similar between the WT and $AR^{-/-}$ mice, and no significant difference was observed in the a-wave, b-wave amplitudes, and the sum of OPs (from OP2 to OP4) amplitudes between WT and $AR^{-/-}$ mice (Fig. 1c). In OIR, a-wave, b-wave, and Ops amplitudes were decreased significantly in WT but not $AR^{-/-}$ mice (Fig. 1c). $AR^{-/-}$ mice appeared to display better preserved ERG waveform than that in WT OIR mice (Fig. 1c). Delayed implicit time (time-to-peak) for a-wave was observed in both genotypes (Fig. 1d). These observations suggested that inner retinal functions were disturbed in OIR and partially preserved with AR deficiency.

To further understand if AR deficiency protects the retinal functions in mouse OIR through preserving retinal neuronal structures, investigation on cellular levels of retinal neurons
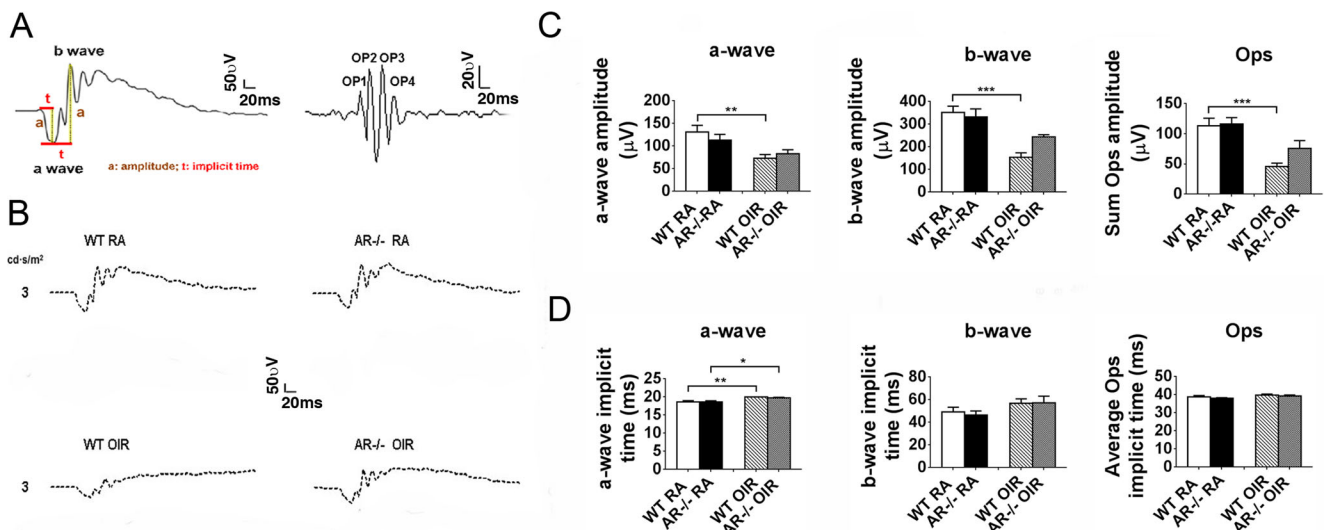
Fig. 1 ERG responses of WT and AR$^{-/-}$ mice on P30. The normal ERG responses with parameters that are usually measured for electrodiagnosis (**a**). Representative ERG waveforms were exhibited at low light intensity (3 cd·s/m^2, dotted line) for both genotypes (**b**). No significant difference was observed in a-wave amplitudes between WT OIR and AR$^{-/-}$ OIR mice. Significantly reduced amplitudes of a-wave, b-wave, and the sum of OPs were found in WT OIR mice but not is AR$^{-/-}$ OIR mice (**c**). The delayed implicit time of a-wave was observed in both genotypes (D). ***$p<0.001$, **$p<0.01$, *$p<0.05$, One-way ANOVA and Bonferroni's multiple comparisons test. $n=5–9$ for each group

was conducted. Retinal thickness was measured and immunohistochemistry for the inner retinal cells was analyzed and compared.

Retinal layer thickness on P17 and P30

Hyperoxia exposure from P7 to P12 induces retinal blood vessel regression and the relative hypoxia-induced neovascularization reaches the maximum on P17 [30]. Therefore, besides P30, the relative hypoxia-induced retinal neuronal changes were also investigated on P17 corresponding to the retinal vascular changes in OIR.

The ONL, INL, and IPL thicknesses in central (~100 μm away from the optic nerve) and the mid-peripheral retinal areas (the middle area between the optic nerve and the end of the retina on either side of the optic nerve) were measured on H&E-stained retinal sections on P17 and P30 (Fig. 2a–b). The central retinal areas are vaso-obliterated while the mid-peripheral areas are the boundary between vaso-obliterated and peripheral areas where neovascularization occurred in the mouse OIR retina. The results were analyzed and compared between WT and AR$^{-/-}$ retinae. Generally, comparable retinal thicknesses at different layers were observed in both WT and AR$^{-/-}$ retinae at room air conditions (Fig. 2c). After OIR, there was no significant change in ONL thickness, but markedly reduced INL and IPL thickness in the central retinal areas were observed versus room-air groups on P17, 30 in both WT and AR$^{-/-}$ retinae (Fig. 2c). More importantly, the reductions in INL and IPL thickness in the mid-peripheral areas observed in WT mice on P17 after OIR were not

observed with AR deficiency. In addition, thicker INL and IPL with AR deficiency were also detected on P30 (Fig. 2c).

Inner retinal neurons on P17 and P30

Horizontal cells Calbindin has been used as a marker for horizontal cells [34, 35]. The immunoreactivity of calbindin is present in cell bodies, dendrites, and axons of horizontal cells along the outer margin of INL [34]. In addition, amacrine cells and RGCs also appeared to be positive for calbindin staining [34]. Here, we focused on the calbindin-positive horizontal cells only.

On P17, evidently located calbindin-positive cell bodies along the outer margin of INL and faintly stained processes between horizontal cells were observed in both genotypes under room air, no significant difference was shown between the two genotypes based on the IHC scoring system (Fig. 3a–b). In OIR, the intensity of calbindin immunoreactivity along outer INL was decreased especially in the processes between horizontal cells in WT but not AR$^{-/-}$ OIR retinae (Fig. 3c–d), although IHC scoring system did not show a significant difference (Fig. 3i). On P30, strong staining of calbindin was exhibited in horizontal cell bodies along the outer margin of INL and processes between the cell bodies in both genotypes under room air (Fig. 3e–f), indicating matured horizontal cell interactions. In OIR, the intensity of calbindin immunoreactivity was decreased in WT retinae but not in AR$^{-/-}$ retinae, and the calbindin staining intensity was significantly stronger in AR$^{-/-}$ retinae than that in WT retinae (Fig. 3g–i). In addition, in AR$^{-/-}$ OIR retinae, cell processes appeared to be more
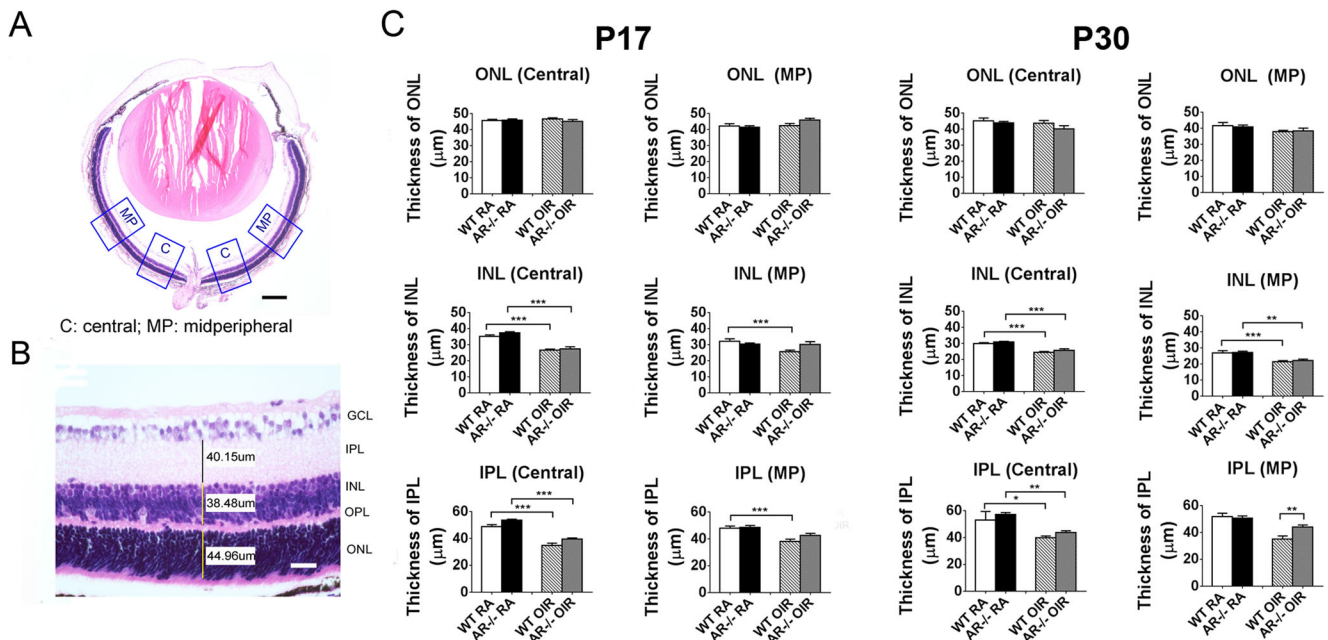
Fig. 2 Retinal thickness in the OIR model and WT mice. Measurement of ONL, INL, and IPL thicknesses in the central and mid-peripheral areas on H&E-stained retinal sections (**a**–**b**). In the central and mid-peripheral retinal area, comparable ONL, INL, and IPL thickness was found in both genotypes on P17 and P30 under room-air and OIR conditions (**c**). Significantly reduced INL and IPL thickness was observed in WT OIR mice (**c**). Significantly thicker IPL in mid-peripheral areas on P30 were observed in AR$^{-/-}$ OIR retinae (**c**). No significant change was observed in ONL thickness (**c**). ***$p<0.001$, **$p<0.01$, *$p<0.05$, One-way ANOVA and Bonferroni's multiple comparisons test. $n=6$–13 for each group. *C* central, *MP* mid-peripheral, *GCL* ganglion cell layer, *IPL* inner plexiform layer, *INL* inner nuclear layer, *OPL* outer plexiform layer, *ONL* outer nuclear layer. Scale bar: 100 μm (**a**); 25 μm (**b**)

strongly calbindin-stained between horizontal cells when compared with WT OIR retinae (Fig. 3h).

Rod bipolar cells PKCα was used for the rod bipolar cells examination. PKCα immunoreactivity was present not only in
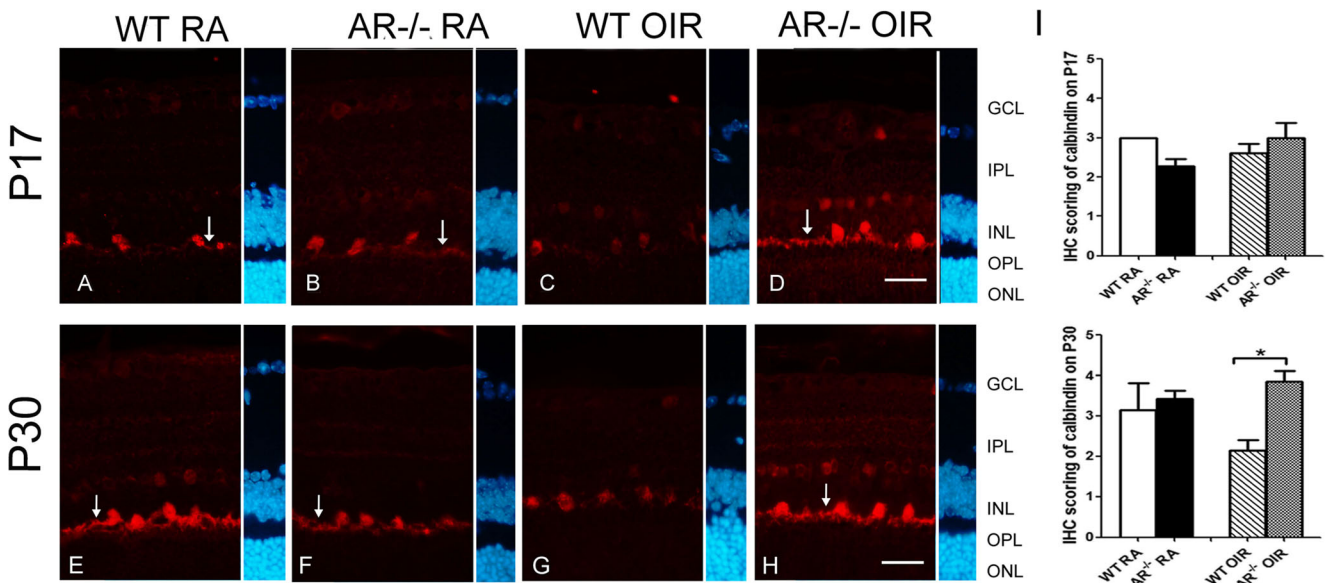

Fig. 3 Evaluation of retinal horizontal cells in the OIR model and WT mice. Immunohistochemical staining of horizontal cells with an antibody against calbindin on P17 and P30 (*red*, **a**–**h**). Calbindin-positive horizontal cell bodies were present along the outer margin of INL in WT and AR$^{-/-}$ RA retinae (**a**–**b**, **e**–**f**). After OIR, reduced calbindin immunoreactivity was observed in WT but not AR$^{-/-}$ OIR retinae (**c**–**d**, **g**–**h**). A trend of calbindin immunoreactivity reduction was also exhibited in WT OIR retinae on P30 (**i**). Significantly more intense calbindin immunoreactivity was observed in AR$^{-/-}$ OIR retinae versus WT OIR retinae on P30 (**i**). The sections were counterstained with DAPI for nuclei identification (*blue*). Arrows, calbindin-positive horizontal cell processes. *$p<0.05$, Kruskal-Wallis test, and Dunn's multiple comparison test. $n=$ 5–9 for each group. Scale bar, 25 μm

the rod bipolar cell bodies along the outer margin of INL but also in their processes extended into IPL. In addition, a few amacrine cells along the inner margin of INL were also stained with PKCα [34–36]. Here, we focused on PKCα-positive rod bipolar cells.

On P17, normally, PKCα immunoreactivity was present in rod bipolar cell bodies in the outer margin of INL and processes close to GCL (Fig. 4a–d). Strong PKCα immunoreactivity was observed in rod bipolar cells for WT and AR$^{-/-}$ room-air retinae (Fig. 4a and b). However, in OIR, a sharp decrease in PKCα immunoreactivity especially in the processes was observed in both genotypes (Fig. 4c and d). The IHC scoring system demonstrated significantly decreased PKCα immunoreactivity in both genotypes in OIR versus room-air controls (Fig. 4i). On P30, PKCα immunoreactivity was apparently exhibited in rod bipolar cell bodies along the outer margin of INL and processes close to GCL in both genotypes under room air (Fig. 4e and f). In OIR, PKCα immunoreactivity, particularly in the processes, was much reduced in WT retinae but not in AR$^{-/-}$ retinae (Fig. 4g and h). The IHC scoring system also showed a significant decrease in WT OIR retinae (Fig. 4i).

Amacrine cells Calretinin was used as a marker for amacrine cells. Calretinin immunoreactivity was observed in the amacrine cell bodies along the inner margin of INL and the three strata of the axon terminals in IPL, as well as some displaced amacrine cells in GCL [34, 35]. In addition, some RGCs were also stained with calretinin [34]. Here, we focused on calretinin-positive amacrine cells in INL as well as three strata in IPL.

On P17, calretinin immunoreactivity was strong in cell bodies in INL and three clear strata in IPL in both genotypes under room air (Fig. 5a and b). In OIR, markedly reduced intensity of calretinin immunoreactivity, seriously distorted three strata in IPL, and decreased cell bodies in INL were observed in WT retinae but not in AR$^{-/-}$ retinae (Fig. 5c and d). The number of calretinin-positive cell bodies along the inner margin of INL was quantified and a significant reduction was shown in WT OIR retinae but not AR$^{-/-}$ OIR retinae (Fig. 5i). On P30, calretinin immunoreactivity was similar to that on P17 in room air controls (Fig. 5e and f). In OIR, the intensity of calretinin immunoreactivity was similar in both genotypes (Fig. 5g and h). A significantly reduced number of cell bodies was observed in WT not AR$^{-/-}$ OIR retinae (Fig. 5i).

RGCs Tuj1 was highly reactive to neuron specific Class III β-tubulin and was, therefore, used as a marker for RGCs [37, 38]. Yet, Tuj1 immunoreactivity was observed not only in cell bodies along GCL but also those in INL (Fig. 6a). In addition, Tuj1 immunoreactivity was also present in the nerve fiber
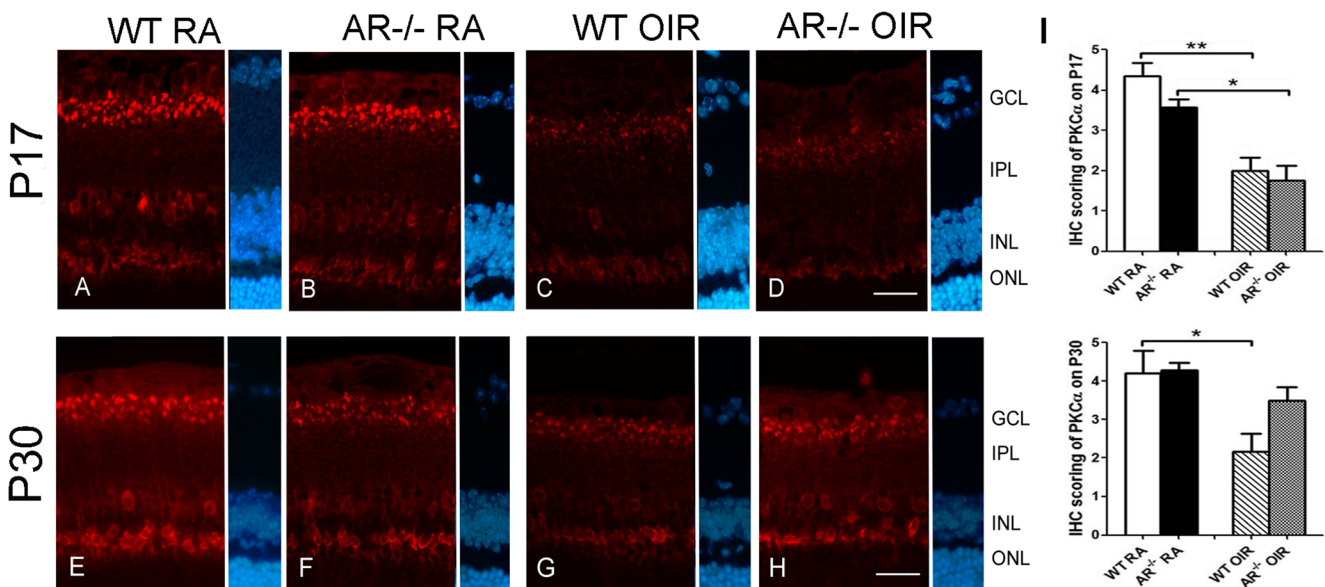

Fig. 4 Evaluation of retinal rod bipolar cells in the OIR model and WT mice. Immunohistochemical staining of rod bipolar cells with an antibody against PKCα on P17 and P30 (*red*, **a**–**h**). PKCα immunoreactivity was present in rod bipolar cell bodies along the outer margin of INL and processes close to GCL in both WT and AR$^{-/-}$ RA retinae (**a**–**b**, **e**–**f**). After OIR, on P17, less PKCα immunoreactivity in rod bipolar cell processes adjacent to GCL was found (**c**–**d**) and significantly reduced PKCα immunoreactivity after OIR was observed in both genotypes (**i**). On P30, significantly reduced PKCα immunoreactivity, particularly in the processes, was observed in WT versus AR$^{-/-}$ OIR retinae (**g**–**h**). The sections were counterstained with DAPI for nuclei identification (*blue*). **$p<0.01$, *$p<0.05$, Kruskal-Wallis test, and Dunn's multiple comparison test. $n=5$–10 for each group. Scale bar, 25 μm
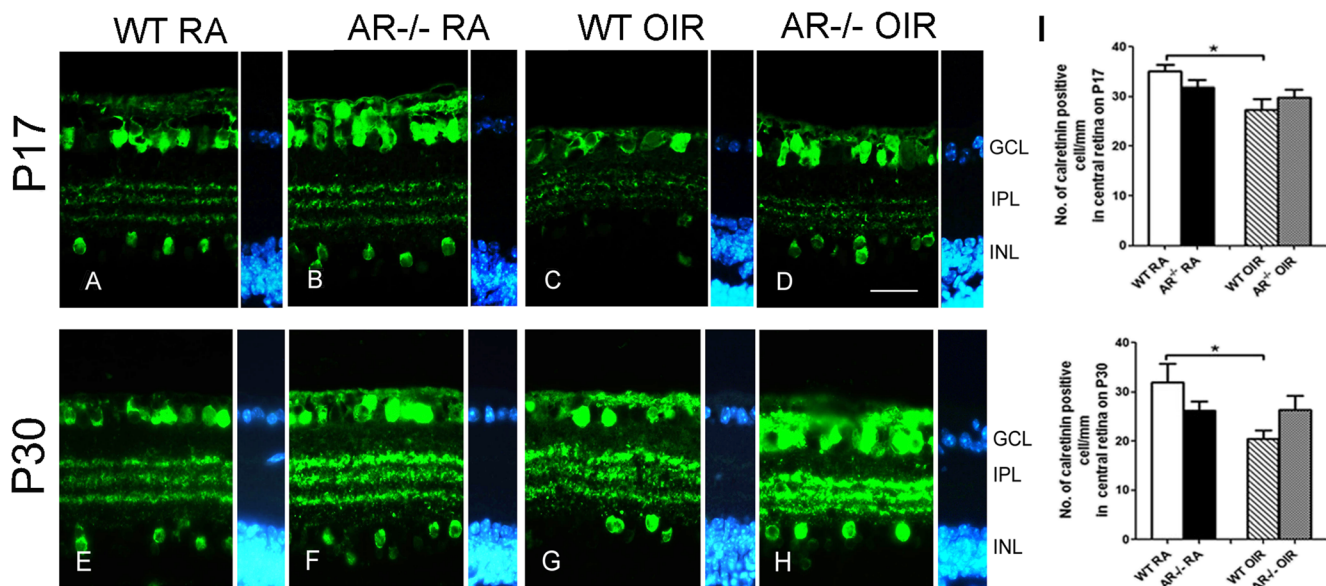
Fig. 5 Evaluation of retinal amacrine cells in the OIR model and WT mice. Immunohistochemical staining of amacrine cells with an antibody against calretinin on P17 and P30 (*green*, **a–h**). Calretinin was expressed in amacrine cell bodies in the innermost layer of INL as well as in three clear and straight strata inside IPL in both WT and AR$^{-/-}$ RA retinae (**a–b**, **e–f**). After OIR, on P17, three distorted strata in IPL were observed especially in WT OIR retinae (**c–d**) and significantly reduced amacrine cells were shown in WT but not AR$^{-/-}$ OIR retinae (**i**). On P30, significantly reduced amacrine cells in INL were only observed in WT OIR retinae (**g–h**, **i**). The sections were counterstained with DAPI for nuclei identification (*blue*). *$p<0.05$, One-way ANOVA, and Bonferroni's multiple comparison test. $n=5$–12 for each group. Scale bar, 25 μm

layer (Fig. 6a). Therefore, Tuj1-positive cell bodies along GCL were regarded as RGCs only when they were also DAPI-positive in merged images (Fig. 6a–c). The number of the Tuj1- and DAPI- positive cells in GCL was quantified and compared between the two genotypes with or without oxygen exposure. Under room-air conditions, a comparable number of RGCs was found in WT and AR-deficient retinae on P17 and P30. No significant difference was observed on P17 and P30 between the two genotypes (Fig. 6d).
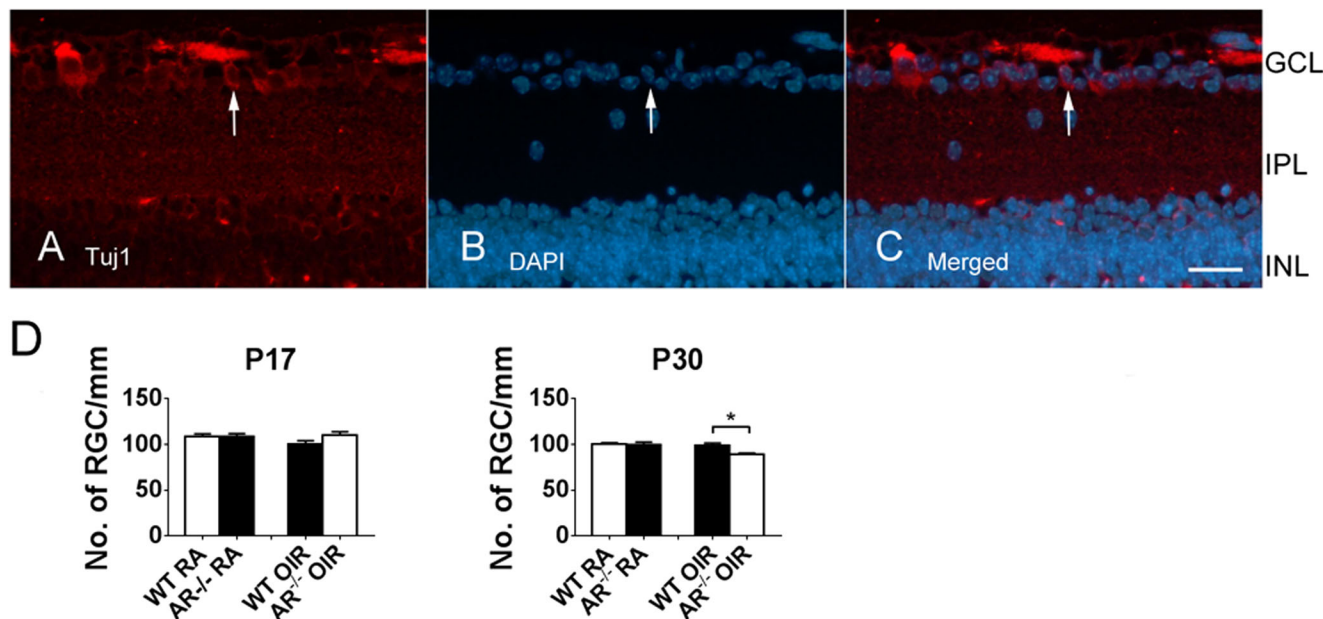

Fig. 6 Evaluation of retinal RGCs in the OIR model and WT mice. Immunohistochemical staining of RGCs with Tuj1 (*red*) and DAPI (*blue*, **a–c**). Only cells positive for both Tuj1 and DAPI were regarded as RGCs (*arrows*, **a–c**). No significant changes in the number of RGCs were observed between WT and AR$^{-/-}$ retinae under room air and after oxygen exposure on P17 and P30 (D). *$p<0.05$, One-way ANOVA and Bonferroni's multiple comparisons test. $n=5$–9 for each group. Scale bar, 25 μm

Müller cell gliosis on P17 and P30

GFAP is a known hallmark of reactive gliosis in astrocytes and Müller cells [39]. Normally, GFAP staining was localized in astrocytes around the blood vessels along the inner limiting membrane (ILM) on P17 and P30 (Fig. 7a and b, e and f). On P17, more intense GFAP immunoreactivity in astrocytes was observed in ILM in WT OIR retinae than that in AR$^{-/-}$ OIR retinae (Fig. 7c and d). Strong GFAP immunoreactivity was also observed in Müller cell processes across IPL (Fig. 7c). In AR$^{-/-}$ OIR retinae, increased GFAP immunoreactivity was also found in ILM (Fig. 7d). Furthermore, less GFAP immunoreactivity in Müller cell processes was observed when compared with WT OIR retinae (Fig. 7d). IHC scoring demonstrated significant GFAP induction in WT but not AR$^{-/-}$ OIR retinae (Fig. 7i). On P30, after OIR, GFAP immunoreactivity was found to be increased in ILM in both genotypes (Fig. 7g and h). In addition, strong GFAP staining was exhibited in some cell processes across IPL in WT OIR retinae (Fig. 7g). However, in AR$^{-/-}$ OIR retinae, only faint GFAP immunoreactivity was shown in Müller cell processes across IPL (Fig. 7h). IHC scoring also revealed a significant increase in GFAP immunoreactivity in WT but not AR$^{-/-}$ OIR retinae (Fig. 7).

Discussion

ROP is well characterized by abnormal vasculature including blood vessel regression and pathological angiogenesis [2]. In addition, ROP also results in retinal neuronal dysfunction [5, 6]. Our results not only compensated current limited studies of hypoxia-induced retinal neuronal changes at the cellular level in the mouse model of OIR, but also demonstrated a potential protective role of AR deficiency in hypoxic retinal neurons in OIR.

Retinal dysfunction has been reported in infants and children with a history of ROP as well as in animal models of OIR [5–14]. ERG was performed to identify retinal function in mice. In ERG recordings, an a-wave is directly produced by photoreceptor cells and a b-wave mainly reflects bipolar and Müller cell functions [40–42]. The OPs are regarded as primarily amacrine cell responses to the light, although ganglion cells are also involved in the generation of Ops [41–43]. It has been demonstrated that a-wave, b-wave, and OPs were all decreased in the animal model of OIR [41, 42, 44]. Our results also exhibited decreased a-wave, b-wave, and OPs amplitudes in WT OIR retinae versus WT room-air retinae. Interestingly, AR deficiency attenuated the reduced ERG responses (b-wave and OPs) observed in WT OIR retinae, suggesting that AR deficiency may help improve the inner retinal function in OIR.

Altered retinal neuronal function suggests related retinal structural changes [5, 7–9, 13, 14, 45]. In the current study, hypoxia-induced phenotypic changes in horizontal cells, amacrine cells, and rod bipolar cells were observed on P17 and P30 in the mouse model of OIR. Previously, morphological changes of horizontal cells, amacrine cells, and rod bipolar cells on P17 have been shown in the mouse model of OIR [3, 12]. Our observations demonstrated that the changes of
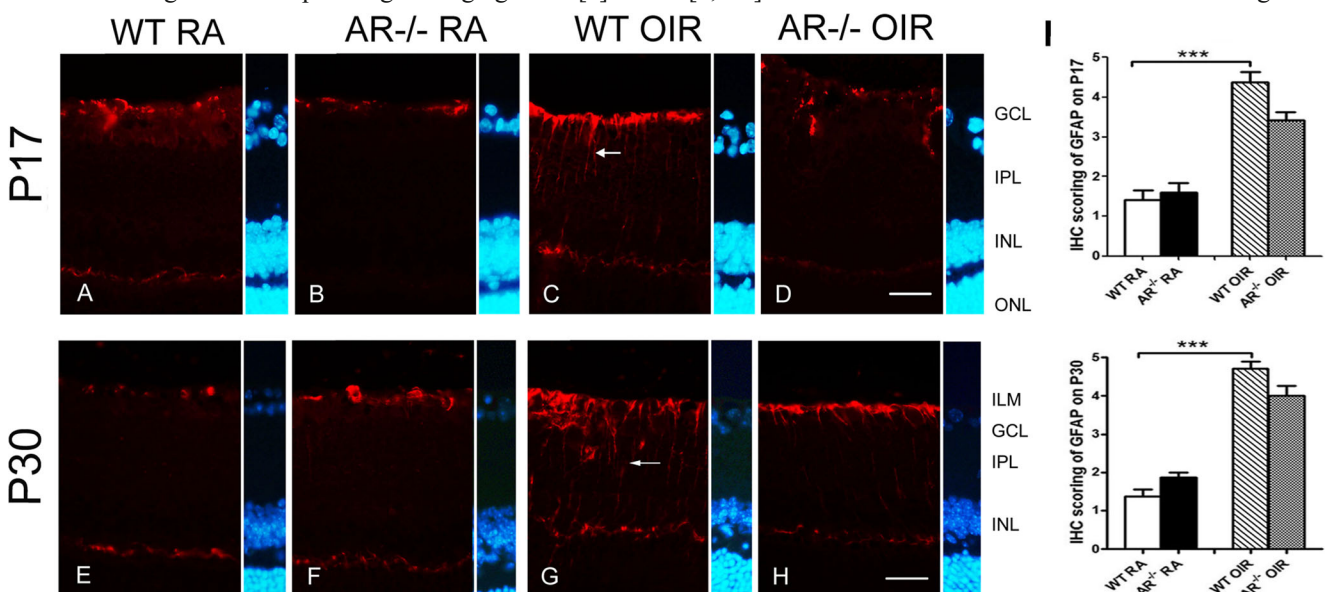

Fig. 7 Evaluation of glial response in the OIR model and WT mice. Immunohistochemical staining of astrocytes and Müller cells with GFAP antibody on P17 and P30 (*red* **a–h**). GFAP immunoreactivity was present in astrocytes along ILM in RA controls for both genotypes (**a–b**, **e–f**). Increased GFAP intensity along ILM was observed in OIR groups versus RA controls for both genotypes (**c–d**, **g–h**). On P17 and P30, intense GFAP immunoreactivity was present in the Müller cell process (arrows) across IPL in WT but not AR$^{-/-}$ OIR retinae (**c–d**, **g–h**). The IHC scoring system also demonstrated significantly increased GFAP induction in WT but not AR$^{-/-}$ OIR retinae (I). The sections were counterstained with DAPI for nuclei identification (*blue*). ***$p < 0.001$, Kruskal-Wallis test, and Dunn's multiple comparison test. $n = 5$–10 for each group. Scale bar, 25 μm

retinal layer thickness and retinal neural cells observed on P17 persist until P30 when the retinal vasculature resolved, suggesting that the protection of retinal neurons should also be considered while targeting the retinal neovascularization in OIR.

With AR deficiency, attenuated changes in horizontal cells and amacrine cells on P17 and P30 as well as rod bipolar cells on P30 were observed when compared with WT OIR retinae. However, no significant change was observed in RGCs on all time points. In fact, previous reports have shown the majority of cell apoptosis on P14 was in INL but not in GCL in the mouse model of OIR [3]. It has been demonstrated that exposure of neonatal rats during the period undergoing significant maturation exhibited more severe damage in the model of OIR [46]. In the neonatal mouse retina, retinal neuronal maturation proceeded from the inner to outer retina with RGCs maturing first [47]. Our observed minimal effects of hypoxia on RGCs, significant effects on horizontal cells, amacrine cells, and rod bipolar cells, agreed well with this maturation process.

Glial responses have been reported in the animal models of OIR [29, 48]. Normally, retinal glia including astrocytes and Müller cells provide the support and nutrients for retinal neurons, maintain the blood retinal barrier (BRB), and function as a template to guide the developing retinal vasculature and neurons in normal conditions [4, 49]. In pathological circumstances, retinal glia became activated and resulted in "reactive gliosis" with GFAP up-regulation [29, 39, 50]. According to previous findings, Müller cell gliosis may contribute to neovascularization and neuronal cell death [48, 51]. Our results showed persistent GFAP induction on P17 and P30 in WT OIR retinae. With AR deficiency, Müller cell gliosis was found to be weaker on P17 and P30 when compared with WT OIR retinae. Therefore, reduced Müller cell gliosis with AR deficiency might contribute to the preserved inner retinal neuronal protection on a respective time point in the mouse model of OIR.

In addition, oxidative stress has also been highly implicated in the pathogenesis of OIR [52, 53]. Animal studies for ROP using antioxidants such as NADPH oxidase inhibitor [52], vitamin E [54], inducible nitric oxide synthase, or cyclooxygenase-2 inhibitors [55] have been found to reduce the progression of OIR. Previously, we have found induced oxidative stress in OIR and AR deficiency could reduce oxidative stress induction in the OIR retinae, especially in the inner nuclear layer and ganglion cell layer [27]. Reduced oxidative stress in the protected inner retinal neurons was observed with AR deficiency, suggesting a direct effect of AR on retinal inner neurons via oxidative stress modulation. Although oxidative stress were shown in GCL, no significant change in the number of RGCs was found, possibly due to the early maturation of RGCs with clearly evident RGC classes observed around P12, and matured RGCs may have more resistance to stressed environment [46, 56].

On P17 and P30, significant reductions in inner retinal thickness were observed in WT OIR retinae in both central and mid-peripheral areas, corresponding to vaso-obliteration and neovascularization in mouse OIR retinae [27, 29, 30, 57–61], respectively. AR deficiency appears to attenuate these reductions in INL and IPL thicknesses especially in the mid-peripheral neovascular areas. Previously, we have shown that genetic deletion of AR reduced neovascularization [27]. As the retinal vasculature supports the retinal neurons with nutrients and oxygen, there is, therefore, a possibility that the attenuated pathological neovascularization with AR deficiency may contribute to the functional and morphological preservation of inner retinal neurons. Further confirmation of the definitive and sequential roles of protected retinal vasculature and preserved retinal neurons with AR deficiency in OIR can be achieved by neuron-specific adeno-associated viral down-regulation of AR expression in retinal neurons.

On P17, our previous observations demonstrated reduced vaso-obliterated areas and neovascular areas in AR$^{-/-}$ OIR retinae [27], suggesting AR deficiency helps protect the normal vascular development as well as inhibit the pathological vessel proliferation. With the known persistent retinal neuronal dysfunction in ROP infants and animal models, further investigation on retinal neuronal changes and stress-responded gliosis were conducted in the current study. Induced gliosis as well as morphological and functional changes of retinal neurons were observed in OIR. AR deficiency demonstrated attenuated gliosis and neuronal abnormalities. Overall, these findings indicated that AR could be considered as a potentially therapeutic target in ROP benefiting both retinal vasculature and neurons, possibly through attenuating glial activation.

References

1. Terry TL (1942) Fibroblastic overgrowth of persistent tunica vasculosa lentis in infants born prematurely: II. Report of cases-clinical aspects. Trans Am Ophthalmol Soc 40:262–284

2. Good WV, Hardy RJ, Dobson V, Palmer EA, Phelps DL, Quintos M, Tung B (2005) The incidence and course of retinopathy of prematurity: findings from the early treatment for retinopathy of

prematurity study. Pediatrics 116:15–23. doi:10.1542/peds.2004-1413

3. Narayanan SP, Suwanpradid J, Saul A, Xu Z, Still A, Caldwell RW, Caldwell RB (2011) Arginase 2 deletion reduces neuro-glial injury and improves retinal function in a model of retinopathy of prematurity. PLoS ONE 6:e22460. doi:10.1371/journal.pone.0022460

4. Vessey KA, Wilkinson-Berka JL, Fletcher EL (2011) Characterization of retinal function and glial cell response in a mouse model of oxygen-induced retinopathy. J Comp Neurol 519:506–527. doi:10.1002/cne.22530

5. Fletcher EL, Downie LE, Hatzopoulos K, Vessey KA, Ward MM, Chow CL, Pianta MJ, Vingrys AJ, Kallioniatis M, Wilkinson-Berka JL (2010) The significance of neuronal and glial cell changes in the rat retina during oxygen-induced retinopathy. Doc Ophthalmol 120:67–86. doi:10.1007/s10633-009-9193-6

6. O'Connor AR, Stephenson T, Johnson A, Tobin MJ, Moseley MJ, Ratib S, Ng Y, Fielder AR (2002) Long-term ophthalmic outcome of low birth weight children with and without retinopathy of prematurity. Pediatrics 109:12–18

7. Fulton AB, Hansen RM (1996) Photoreceptor function in infants and children with a history of mild retinopathy of prematurity. J Opt Soc Am A Opt Image Sci Vis 13:566–571

8. Hansen RM, Harris ME, Moskowitz A, Fulton AB (2010) Deactivation of the rod response in retinopathy of prematurity. Doc Ophthalmol 121:29–35. doi:10.1007/s10633-010-9228-z

9. Harris ME, Moskowitz A, Fulton AB, Hansen RM (2011) Long-term effects of retinopathy of prematurity (ROP) on rod and rod-driven function. Doc Ophthalmol 122:19–27. doi:10.1007/s10633-010-9251-0

10. Fulton AB, Hansen RM, Moskowitz A (2009) Development of rod function in term born and former preterm subjects. Optom Vis Sci 86:E653–E658. doi:10.1097/OPX.0b013e3181a6a237

11. Fulton AB, Hansen RM, Moskowitz A, Barnaby AM (2005) Multifocal ERG in subjects with a history of retinopathy of prematurity. Doc Ophthalmol 111:7–13. doi:10.1007/s10633-005-2621-3

12. Liang X, Zhou H, Ding Y, Li J, Yang C, Luo Y, Li S, Sun G, Liao X, Min W (2012) TMP prevents retinal neovascularization and imparts neuroprotection in an oxygen-induced retinopathy model. Invest Ophthalmol Vis Sci 53:2157–2169. doi:10.1167/iovs.11-9315

13. Liu K, Akula JD, Falk C, Hansen RM, Fulton AB (2006) The retinal vasculature and function of the neural retina in a rat model of retinopathy of prematurity. Invest Ophthalmol Vis Sci 47:2639–2647. doi:10.1167/iovs.06-0016

14. Reynaud X, Hansen RM, Fulton AB (1995) Effect of prior oxygen exposure on the electroretinographic responses of infant rats. Invest Ophthalmol Vis Sci 36:2071–2079

15. Chen J, Stahl A, Hellstrom A, Smith LE (2011) Current update on retinopathy of prematurity: screening and treatment. Curr Opin Pediatr 23:173–178. doi:10.1097/MOP.0b013e3283423f35

16. Clark D, Mandal K (2008) Treatment of retinopathy of prematurity. Early Hum Dev 84:95–99. doi:10.1016/j.earlhumdev.2007.11.007

17. Harder BC, von Baltz S, Jonas JB, Schlichtenbrede FC (2011) Intravitreal bevacizumab for retinopathy of prematurity. J Ocul Pharmacol Ther 27:623–627. doi:10.1089/jop.2011.0060

18. Davis JM, Auten RL (2010) Maturation of the antioxidant system and the effects on preterm birth. Semin Fetal Neonatal Med 15:191–195. doi:10.1016/j.siny.2010.04.001

19. Quinn GE, Johnson L, Otis C, Schaffer DB, Bowen FW (1990) Incidence, severity and time course of ROP in a randomized clinical trial of vitamin E prophylaxis. Doc Ophthalmol 74:223–228

20. Cheung AK, Lo AC, So KF, Chung SS, Chung SK (2007) Gene deletion and pharmacological inhibition of aldose reductase protect against retinal ischemic injury. Exp Eye Res 85:608–616. doi:10.1016/j.exer.2007.07.013

21. Chung SS, Ho EC, Lam KS, Chung SK (2003) Contribution of polyol pathway to diabetes-induced oxidative stress. J Am Soc Nephrol 14:S233–S236

22. Lee AY, Chung SS (1999) Contributions of polyol pathway to oxidative stress in diabetic cataract. FASEB J 13:23–30

23. Lou MF, Dickerson JE Jr, Garadi R, York BM Jr (1988) Glutathione depletion in the lens of galactosemic and diabetic rats. Exp Eye Res 46:517–530

24. Obrosova IG (2005) Increased sorbitol pathway activity generates oxidative stress in tissue sites for diabetic complications. Antioxid Redox Signal 7:1543–1552. doi:10.1089/ars.2005.7.1543

25. Obrosova IG, Pacher P, Szabo C, Zsengeller Z, Hirooka H, Stevens MJ, Yorek MA (2005) Aldose reductase inhibition counteracts oxidative-nitrosative stress and poly(ADP-ribose) polymerase activation in tissue sites for diabetes complications. Diabetes 54:234–242

26. Song Z, Fu DT, Chan YS, Leung S, Chung SS, Chung SK (2003) Transgenic mice overexpressing aldose reductase in Schwann cells show more severe nerve conduction velocity deficit and oxidative stress under hyperglycemic stress. Mol Cell Neurosci 23:638–647

27. Fu ZJ, Li SY, Kociok N, Wong D, Chung SK, Lo AC (2012) Aldose reductase deficiency reduced vascular changes in neonatal mouse retina in oxygen-induced retinopathy. Invest Ophthalmol Vis Sci 53:5698–5712. doi:10.1167/iovs.12-10122

28. Ho HT, Chung SK, Law JW, Ko BC, Tam SC, Brooks HL, Knepper MA, Chung SS (2000) Aldose reductase-deficient mice develop nephrogenic diabetes insipidus. Mol Cell Biol 20:5840–5846

29. Smith LE, Wesolowski E, McLellan A, Kostyk SK, D'Amato R, Sullivan R, D'Amore PA (1994) Oxygen-induced retinopathy in the mouse. Invest Ophthalmol Vis Sci 35:101–111

30. Connor KM, Krah NM, Dennison RJ, Aderman CM, Chen J, Guerin KI, Sapieha P, Stahl A, Willett KL, Smith LE (2009) Quantification of oxygen-induced retinopathy in the mouse: a model of vessel loss, vessel regrowth and pathological angiogenesis. Nat Protoc 4:1565–1573. doi:10.1038/nprot.2009.187

31. Akula JD, Mocko JA, Moskowitz A, Hansen RM, Fulton AB (2007) The oscillatory potentials of the dark-adapted electroretinogram in retinopathy of prematurity. Invest Ophthalmol Vis Sci 48:5788–5797. doi:10.1167/iovs.07-0881

32. Li SY, Yang D, Fu ZJ, Woo T, Wong D, Lo AC (2012) Lutein enhances survival and reduces neuronal damage in a mouse model of ischemic stroke. Neurobiol Dis 45:624–632. doi:10.1016/j.nbd.2011.10.008

33. Yang D, Li SY, Yeung CM, Chang RC, So KF, Wong D, Lo AC (2012) Lycium barbarum extracts protect the brain from blood–brain barrier disruption and cerebral edema in experimental stroke. PLoS ONE 7, e33596. doi:10.1371/journal.pone.0033596

34. Haverkamp S, Wassle H (2000) Immunocytochemical analysis of the mouse retina. J Comp Neurol 424:1–23

35. Li SY, Fu ZJ, Ma H, Jang WC, So KF, Wong D, Lo AC (2009) Effect of lutein on retinal neurons and oxidative stress in a model of acute retinal ischemia/reperfusion. Invest Ophthalmol Vis Sci 50:836–843. doi:10.1167/iovs.08-2310

36. Morrow EM, Chen CM, Cepko CL (2008) Temporal order of bipolar cell genesis in the neural retina. Neural Dev 3:2. doi:10.1186/1749-8104-3-2

37. Robinson GA, Madison RD (2004) Axotomized mouse retinal ganglion cells containing melanopsin show enhanced survival, but not enhanced axon regrowth into a peripheral nerve graft. Vis Res 44:2667–2674. doi:10.1016/j.visres.2004.06.010

38. Watanabe M, Rutishauser U, Silver J (1991) Formation of the retinal ganglion cell and optic fiber layers. J Neurobiol 22:85–96. doi:10.1002/neu.480220109

39. Pekny M, Nilsson M (2005) Astrocyte activation and reactive gliosis. Glia 50:427–434. doi:10.1002/glia.20207

40. Miller RF, Dowling JE (1970) Intracellular responses of the Muller (glial) cells of mudpuppy retina: their relation to b-wave of the electroretinogram. J Neurophysiol 33:323–341

41. Nakamura S, Imai S, Ogishima H, Tsuruma K, Shimazawa M, Hara H (2012) Morphological and functional changes in the retina after chronic oxygen-induced retinopathy. PLoS ONE 7:e32167. doi:10.1371/journal.pone.0032167

42. Dal Monte M, Latina V, Cupisti E, Bagnoli P (2012) Protective role of somatostatin receptor 2 against retinal degeneration in response to hypoxia. Naunyn Schmiedeberg's Arch Pharmacol 385:481–494. doi:10.1007/s00210-012-0735-1

43. Wachtmeister L (1998) Oscillatory potentials in the retina: what do they reveal. Prog Retin Eye Res 17:485–521

44. Mowat FM, Gonzalez F, Luhmann UF, Lange CA, Duran Y, Smith AJ, Maxwell PH, Ali RR, Bainbridge JW (2012) Endogenous erythropoietin protects neuroretinal function in ischemic retinopathy. Am J Pathol 180:1726–1739. doi:10.1016/j.ajpath.2011.12.033

45. Fulton AB, Reynaud X, Hansen RM, Lemere CA, Parker C, Williams TP (1999) Rod photoreceptors in infant rats with a history of oxygen exposure. Invest Ophthalmol Vis Sci 40:168–174

46. Dembinska O, Rojas LM, Varma DR, Chemtob S, Lachapelle P (2001) Graded contribution of retinal maturation to the development of oxygen-induced retinopathy in rats. Invest Ophthalmol Vis Sci 42:1111–1118

47. Olney JW (1968) An electron microscopic study of synapse formation, receptor outer segment development, and other aspects of developing mouse retina. Invest Ophthalmol 7:250–268

48. Bai Y, Ma JX, Guo J, Wang J, Zhu M, Chen Y, Le YZ (2009) Müller cell-derived VEGF is a significant contributor to retinal neovascularization. J Pathol 219:446–454. doi:10.1002/path.2611

49. Dorrell MI, Aguilar E, Jacobson R, Trauger SA, Friedlander J, Siuzdak G, Friedlander M (2010) Maintaining retinal astrocytes normalizes revascularization and prevents vascular pathology associated with oxygen-induced retinopathy. Glia 58:43–54. doi:10.1002/glia.20900

50. Bringmann A, Pannicke T, Grosche J, Francke M, Wiedemann P, Skatchkov SN, Osborne NN, Reichenbach A (2006) Müller cells in the healthy and diseased retina. Prog Retin Eye Res 25:397–424. doi:10.1016/j.preteyeres.2006.05.003

51. Bringmann A, Iandiev I, Pannicke T, Wurm A, Hollborn M, Wiedemann P, Osborne NN, Reichenbach A (2009) Cellular signaling and factors involved in Müller cell gliosis: neuroprotective and detrimental effects. Prog Retin Eye Res 28:423–451. doi:10.1016/j.preteyeres.2009.07.001

52. Al-Shabrawey M, Bartoli M, El-Remessy AB, Platt DH, Matragoon S, Behzadian MA, Caldwell RW, Caldwell RB (2005) Inhibition of NAD(P)H oxidase activity blocks vascular endothelial growth factor overexpression and neovascularization during ischemic retinopathy. Am J Pathol 167:599–607. doi:10.1016/S0002-9440(10)63001-5

53. Lo AC, Cheung AK, Hung VK, Yeung CM, He QY, Chiu JF, Chung SS, Chung SK (2007) Deletion of aldose reductase leads to protection against cerebral ischemic injury. J Cereb Blood Flow Metab 27:1496–1509. doi:10.1038/sj.jcbfm.9600452

54. Penn JS, Tolman BL, Bullard LE (1997) Effect of a water-soluble vitamin E analog, trolox C, on retinal vascular development in an animal model of retinopathy of prematurity. Free Radic Biol Med 22:977–984

55. He T, Xing YQ, Zhao XH, Ai M (2007) Interaction between iNOS and COX-2 in hypoxia-induced retinal neovascularization in mice. Arch Med Res 38:807–815. doi:10.1016/j.arcmed.2007.05.003

56. Coombs JL, Van Der List D, Chalupa LM (2007) Morphological properties of mouse retinal ganglion cells during postnatal development. J Comp Neurol 503:803–814. doi:10.1002/cne.21429

57. Shao Z, Fu Z, Stahl A, Joyal JS, Hatton C, Juan A, Hurst C, Evans L, Cui Z, Pei D, Gong Y, Xu D, Tian K, Bogardus H, Edin ML, Lih F, Sapieha P, Chen J, Panigrahy D, Hellstrom A, Zeldin DC, Smith LE (2014) Cytochrome P450 2C8 omega3-long-chain polyunsaturated fatty acid metabolites increase mouse retinal pathologic neovascularization–brief report. Arterioscler Thromb Vasc Biol 34:581–586. doi:10.1161/ATVBAHA.113.302927

58. Fu Z, Lofqvist CA, Shao Z, Sun Y, Joyal JS, Hurst CG, Cui RZ, Evans LP, Tian K, SanGiovanni JP, Chen J, Ley D, Pupp IH, Hellstrom A, Smith LE (2015) Dietary ω-3 polyunsaturated fatty acids decrease retinal neovascularization by adipose–endoplasmic reticulum stress reduction to increase adiponectin. Am J Clin Nutr 101(4):879–888. doi:10.3945/ajcn.114.099291

59. Li Y, Liu CH, Sun Y, Gong Y, Fu Z, Evans LP, Tian KT, Juan AM, Hurst CG, Mammoto A, Chen J (2014) Endothelial TWIST1 promotes pathological ocular angiogenesis. Invest Ophthalmol Vis Sci 55:8267–8277. doi:10.1167/iovs.14-15623

60. Wang Z, Cheng R, Lee K, Tyagi P, Ding L, Kompella UB, Chen J, Xu X, Ma JX (2015) Nanoparticle-mediated expression of a wnt pathway inhibitor ameliorates ocular neovascularization. Arterioscler Thromb Vasc Biol 35:855–864. doi:10.1161/ATVBAHA.114.304627

61. Wang Z, Moran E, Ding L, Cheng R, Xu X, Ma JX (2014) PPARalpha regulates mobilization and homing of endothelial progenitor cells through the HIF-1alpha/SDF-1 pathway. Invest Ophthalmol Vis Sci 55:3820–3832. doi:10.1167/iovs.13-13396